Strongly mixed resonances in the photofragmentation of HeBr 2 near Br 2 (B) dissociation: Stabilization and close-coupling studies

Tomás González-Lezana, Marta I. Hernández, Gerardo Delgado-Barrio, and Pablo Villarreal

Citation: The Journal of Chemical Physics **106**, 3216 (1997); doi: 10.1063/1.473421
View online: http://dx.doi.org/10.1063/1.473421
View Table of Contents: http://scitation.aip.org/content/aip/journal/jcp/106/8?ver=pdfcov
Published by the AIP Publishing

Strongly mixed resonances in the photofragmentation of $HeBr_2$ near $Br_2(B)$ dissociation: Stabilization and close-coupling studies

Tomás González-Lezana, Marta I. Hernández, Gerardo Delgado-Barrio, and Pablo Villarreal
Instituto de Matemáticas y Física Fundamental (C.S.I.C.), Serrano 123, E-28006-Madrid, Spain

(Received 16 September 1996; accepted 8 November 1996)

The photofragmentation of the $He^{79}Br_2$ van der Waals complex is studied for the transition from the ground to the excited electronic state B and where the Br_2 subunit is also excited to the neighborhood of the $v_0=45$ vibrational state. At this vibrational level the bromine molecule is close to its dissociation limit and the $\Delta v=-1$ channel is closed for dissociation of the complex. In a previous work it was suggested that energy in the $HeBr_2(B,\ v_0=45)$ quasibound state may be internally redistributed (exciting van der Waals modes at the expense of the bromine excitation) prior to dissociation. Such mechanisms are more deeply studied in this work by means of the stabilization method, which works with square-integrable wave functions and is an appropriate approach to perform quasibound state analysis. Stabilization total cross sections compare fairly well with close-coupling ones, where the proper asymptotic behaviour of the continuum wave functions is taken into account. By inspection of the quasibound state wave functions, it is seen that energy is redistributed to several excited states belonging to the v_0-1 manifold. In addition, it is shown that such excited states also carry oscillator strength in the transition from the ground electronic state and thus interference effects in the excitation process are significant. $HeBr_2$ near the halogen dissociation limit is found to be a rather strongly coupled system where the quasibound states involved can only approximately be assigned to quantum numbers corresponding to interhalogen and van der Waals vibrational excitations. © *1997 American Institute of Physics.* [S0021-9606(97)00407-8]

I. INTRODUCTION

Recently, the authors have performed three-dimensional quantum mechanical calculations to study the photofragmentation of the $HeBr_2$ van der Waals (vdW) molecule.[1] The leading process occurring in this complex is vibrational predissociation (VP): a photon promotes the molecular system from the ground (X) to an electronically excited (B) state, also depositing energy into the halogen vibrational motion. After several halogen vibrational periods, energy is transferred to vdW modes and the complex eventually fragmentates. A wide range of initial Br_2 vibrational excitations ($v_0=8-46$) was investigated, using simple additive pairwise Morse potentials for both electronic states. For excitations to vibrational levels $v_0=8$ to $v_0=38$, calculated lifetimes, spectral shifts, average geometries and product average energies compare quite well with the experimental measurements.[2–5] For higher vibrational excitations, where the $Br_2(B)$ diatom is close to dissociation, cross section profiles show complicated structures and, besides, spectral shifts and lifetimes exhibit a ''zig–zag'' dependence on v, suggesting that several quasibound states are strongly interacting. Although agreement with experiments is somewhat poorer in this range of vibrational excitations, calculations do successfully reproduce the closing of the $\Delta v=-1$ channel at $v_0=44$ (the vdW binding energy is larger than the $\Delta v=-1$ bromine level spacing). At $v_0=45$, wherein dissociation can only occur by the loss of two or more vibrational quanta, two resonance peaks of about the same intensity were obtained in the simulated cross sections and, besides, rotational distributions at the maximum of both peaks were found to be fairly similar.

Similar effects have been reported for related rare-gas halogen vdW complexes in the $\Delta v=-2$ regime (where the $\Delta v=-1$ channel is closed). In that situation, a direct mechanism (direct coupling of the initial level to the dissociative continuum) may compete with intramolecular vibrational-energy redistribution (IVR) where energy flows from the halogen vibration to vdW excited modes of the v_0-1 manifold prior to fragmentation. In NeI_2, for instance, an erratic dependence of resonance widths with v_0 was attributed to a configuration interaction effect of a few zero-order quasibound levels.[6] In addition, the $\Delta v=-2$ regime of $ArCl_2$ has been widely studied both experimentally[11] and theoretically.[12–15] Janda and co-workers[11] measured product rotational distributions, finding that they are highly structured and very sensitive to the initial Cl_2 vibrational excitation. IVR mechanisms were proposed to explain the experimental findings and, in this way, the $ArCl_2$ cluster was proposed as an ideal system to investigate IVR phenomena, since very detailed experimental and theoretical studies can be performed for such a relatively simple and small molecule. To explain the experimental findings, Halberstadt *et al.*[12] invoked a sparse IVR model where the quasibound states involved can be written as

$$\Psi_1=\alpha\Psi^0_{v_0,n=0}+\beta\Psi^0_{v_0-1,n\gg 0},$$
$$\Psi_2=-\beta\Psi^0_{v_0,n=0}+\alpha\Psi^0_{v_0-1,n\gg 0}, \tag{1.1}$$

with n labelling the excitation of the vdW modes. The main

 0021-9606/97/106(8)/3216/11/$10.00

assumptions within this model were: a) The $X \rightarrow B$ transition intensity is completely due to the $\Psi^0_{v_0,n=0}$ zero-order state, the ''bright'' state, and b) only the dark state $\Psi^0_{v_0-1,n>>0}$ couples directly to the dissociation continuum. As a consequence, two peaks would appear in the excitation spectra (where the intensities of the transitions to Ψ_1 and Ψ_2 are proportional to α^2 and β^2, respectively). In addition, fragmentation of Ψ_1 or Ψ_2 leads to the same product state distribution since it is dominated by the doorway state $\Psi^0_{v_0-1,n>>0}$. More detailed theoretical works have subsequently appeared where the previous picture has been refined, using both time-independent[13,14] and time-dependent[15] approaches. On the other hand, the $\Delta v=-3$ regime of ArI_2 has been a subject of experimental[7,8] and theoretical[9,10] work, where it has been found that IVR mediates the fragmentation process.

In view of the theoretical findings on the $HeBr_2$ (B, $v_0=$high) dynamics and comparing with $ArCl_2$, one may postulate a similar IVR mechanism in the $\Delta v=-2$ regime of $HeBr_2$. Unfortunately, so far it has not been possible to resolve experimentally final rotational distributions in the latter case. Such measurements could shed light on this hypothetical mechanism. At any rate, a deeper theoretical understanding could be obtained by means of the identification of the most relevant zero-order quasibound states as well as the most important couplings ruling both the excitation and the fragmentation processes. In this context, the stabilization theory of dynamics[16] is an excellent framework for quasibound state analysis, as it allows one to recognize the most important zero-order states involved in a complex-mediated dynamics. Recently, the stabilization theory has undergone a renewed impetus: not only the energies of isolated resonances can be computed using square-integrable ($\mathscr{L}^2$) wave functions, but also the density of states (and thus, resonance widths)[17,18] can be obtained, among many other observables.[19–23] In addition, this method looks very appealing since it basically involves performing standard bound state-like diagonalizations. At this point, it should be mentioned that complex $\mathscr{L}^2$ methods, imposing absorbing boundary conditions, have been successfully applied to simulate cross section profiles.[24] In the context of vdW complexes, stabilization techniques were used in a two-dimensional model of predissociation[25] as well as in VP of NeICl, within the regime of isolated resonances, where also a complex scaling method is employed.[22] As Salzgeber *et al.*[26] pointed out, it would be very interesting to test this method in more and more challenging situations, such as multichannel decay, overlapping of resonances and threshold effects.

In this work we present an application of the stabilization method in a truly non-trivial case, the fragmentation of $HeBr_2(B,\ v_0=45)$, where all the above-mentioned effects are present. Within this approach, the photofragmentation cross section is computed[19] and compared with three-dimensional close-coupling calculations.[1,27] In this way, not only resonance positions and widths but also spectral intensities are obtained. The states causing maximum peaks in the spectrum are identified and studied in terms of their nodal patterns in stretching and bending vibrational modes. A conclusion emerging from this analysis is that, in the region near the Br_2 dissociation limit, resonance states only can be nearly labelled by quantum numbers associated to halogen and vdW vibrational modes, as they result from important mixings of several zero-order states belonging to different v manifolds. In addition to this, and by means of close-coupling calculations, it is shown that not only the $(v=45,\ n=0)$ state carries oscillator strength in the optical transition but other (excited) vdW states belonging to $v \neq 45$ manifolds do also.

The paper is organized as follows. In Section II, the basic equations are presented. Results are reported and discussed in Section III. Finally, a brief conclusion is given in Section IV.

II. THEORY

A. Photofragmentation of rare gas-halogen complexes: overview

The basic quantum theory of photofragmentation of rare-gas halogen complexes is outlined here. A more detailed presentation is given in Ref. 27. Within the first order perturbation theory for electric dipole transitions, the total cross section for excitation from a rovibrational bound state i of the electronic ground state X of $HeBr_2$ is given by

$$\sigma_i(E)=\frac{4\pi^2\omega}{c}\sum_f |\langle \Psi_{fE}(B)|\boldsymbol{\mu}\cdot\mathbf{e}|\Psi_i(X)\rangle|^2, \tag{2.1}$$

where ω and $\mathbf{e}$ are the frequency and polarization vector of the incident photon, respectively, $\boldsymbol{\mu}$ is the transition dipole moment of the system for the $(X \rightarrow B)$ electronic transition, $\Psi_i(X)$ and $\Psi_{fE}(B)$ are bound and dissociative nuclear wave functions with energies E_i and $E=E_i+\hbar\omega$, respectively, and f specifies the quantum numbers of the $Br_2(B)$ fragment.

Both wave functions $\Psi_i(X)$ and $\Psi_{fE}(B)$ are solutions of Hamiltonians of the form:

$$H^{\epsilon}=-\frac{\hbar^2}{2m}\frac{\partial^2}{\partial R^2}-\frac{\hbar^2}{2\mu}\frac{\partial^2}{\partial r^2}+\frac{\mathbf{l}^2}{2mR^2}+\frac{\mathbf{j}^2}{2\mu r^2} + V^{\epsilon}_{Br_2}(r)+W^{\epsilon}_{HeBr_2}(r,R,\theta), \tag{2.2}$$

where Jacobi coordinates are used: $\mathbf{r}$ is the vector joining the two Br nuclei, $\mathbf{R}$ is the vector going from the center of mass of Br_2 to the helium nucleus, and θ is the angle between $\mathbf{r}$ and $\mathbf{R}$. The reduced masses of Br_2 and $HeBr_2$ are μ and m, while $\mathbf{l}$ and $\mathbf{j}$ are angular momenta associated with the vectors $\mathbf{R}$ and $\mathbf{r}$, respectively. $V^{\epsilon}_{Br_2}$ and $W^{\epsilon}_{HeBr_2}$ are intramolecular and vdW intermolecular interaction potentials for the ground ($\epsilon=X$) and excited ($\epsilon=B$) electronic states. Initial and final wave functions are expanded as follows

$$\Psi_i^{J'M'p_i'p_j'}(\boldsymbol{R},r;X) = \sum_{v'k'j'\Omega'} a^i_{v'k'j'\Omega'}\varphi_{k'}(R)\chi^X_{v'}(r)\Theta^{J'M'p_i'p_j'}_{j'\Omega'}(\hat{\mathbf{r}},\hat{\mathbf{R}}), \tag{2.3}$$

$$\Psi^{JMp_ip_j}_{fE}(\boldsymbol{R},r;B) = \sum_{vj\Omega} \phi^{fE}_{vj\Omega}(R)\chi^B_v(r)\Theta^{JMp_ip_j}_{j\Omega}(\hat{\mathbf{r}},\hat{\mathbf{R}}), \tag{2.4}$$

where χ's are eigenfunctions of the effective Hamiltonian $-(\hbar^2/2\mu)(\partial^2/\partial r^2)+V^{\epsilon}_{Br_2}(r)$. On the other hand, $\{\Theta^{JMp_ip_j}_{j\Omega}\}$ is a free rotor basis set,[1,27] where J is the total angular momentum, M and Ω its projections onto the space and body fixed z axes, respectively, p_i is the parity under nuclear coordinates inversion, and p_j is the parity under bromine nuclei exchange ($p_j=+1$ or -1 when the quantum number j is even or odd, respectively). In Eq. (2.3), $\{\varphi_{k'}(R)\}$ are square-integrable functions belonging to an orthonormal basis set. In Eq. (2.4), ϕ's are energy-normalized continuum wave functions.

In rare gas-halogen systems, it is usually assumed that the transition dipole moment $\boldsymbol{\mu}$ [Eq. (2.1)] lies along the halogen axis and, besides, its magnitude is independent of the internuclear distance r. Thus, the total cross section for an allowed transition $J'^{p_i'}_{p_j'}(X)\rightarrow J^{p_i}_{p_j}(B)$ can be written as[27,28]

$$\sigma_i(E)\propto\sum_f \left| \sum_{vj\Omega}\sum_{v'j'\Omega'} \langle \phi^{fE}_{vj\Omega}|\phi^i_{v'j'\Omega'}\rangle F(v',v)G^{(Jj\Omega)}_{(J'j'\Omega')} \right|^2, \tag{2.5}$$

where

$$F(v',v)=\langle\chi^B_v|\chi^X_{v'}\rangle \tag{2.6}$$

are halogen Franck–Condon (FC) factors and

$$\phi^i_{v'j'\Omega'}(R)=\sum_{k'} a^i_{v'k'j'\Omega'}\varphi_{k'}(R), \tag{2.7}$$

$$G^{(Jj\Omega)}_{(J'j'\Omega')} = g_j g_{j'} N_{\Omega'\Omega} \begin{pmatrix} j & 1 & j' \\ 0 & 0 & 0 \end{pmatrix} \times \sum_t \begin{pmatrix} j & 1 & j' \\ -\Omega & t & \Omega' \end{pmatrix} \begin{pmatrix} J & 1 & J' \\ -\Omega & t & \Omega' \end{pmatrix}, \tag{2.8}$$

$$g_j=(2j+1)^{1/2}, \tag{2.9}$$

$$N_{\Omega'\Omega}=(1+|\delta_{\Omega'0}-\delta_{\Omega 0}|)^{1/2}. \tag{2.10}$$

In addition, selection rules for the transition are $p_i' \neq p_i$, $p_j' \neq p_j$, and $\Delta J=0,\pm 1$ ($0\rightarrow 0$ forbidden).

B. The close-coupling method

In the widely used close-coupling method, the expansion given in Eq. (2.4) is introduced into the Schrödinger equation for H^B [Eq. (2.2)] and, after projection onto the basis functions for interhalogen and angular degrees of freedom, a close coupled system for the set of unknown functions $\phi^{fE}_{vj\Omega}(R)$ is obtained.[27] Such close-coupled equations are solved by means of a suitable propagation method,[29] and applying standard boundary conditions for outgoing waves.[27] The quadrature involved in Eq. (2.1) is carried out by accumulation at the same time that the propagation is performed,[30] so the continuum wave functions $\phi^{fE}_{vj\Omega}(R)$ are not explicitly obtained.

C. The stabilization method

The stabilization method uses $\mathscr{L}^2$ (or ''bound state'' type) representations of continuum wave functions which, despite their approximative nature, provide an useful and quite accurate picture of quasibound states involved in scattering resonances. Within this framework, the continuum wave function for the B state [Eq. (2.4)] is written as an expansion of square-integrable basis functions, similar to the expansion used for the bound X-state calculation [Eq. (2.3)] (electronic state labels are dropped for simplicity):

$$\Phi^{JMp_ip_j}_m(\boldsymbol{R},\boldsymbol{r};\alpha) = \sum_{vkj\Omega} b^m_{vkj\Omega}(\alpha)\varphi_k(R;\alpha)\chi_v(r)\Theta^{JMp_ip_j}_{j\Omega}(\hat{\mathbf{r}},\hat{\mathbf{R}}), \tag{2.11}$$

where $\varphi_k(R;\alpha)$ functions above constitute an orthonormal basis set ($\langle\varphi_k|\varphi_{k'}\rangle=\delta_{kk'}$). In the present calculations they are discrete variable representation (DVR) functions obtained from diagonalization of the R-coordinate operator in a primitive harmonic oscillator (HO) basis set with frequency parameter

$$\omega=\sqrt{\alpha}\omega_0, \tag{2.12}$$

where ω_0 is a reference frequency and α is a dimensionless scale factor. By decreasing α, for instance, the DVR basis set expands a larger region in the R-coordinate space (since a smaller ω in the HO basis gives more spreaded DVR eigenvalues). For a given value of α, a set of discretized continuum wave functions $\Phi_m(\alpha)$ and the associated eigenvalues $E_m(\alpha)$ are obtained from diagonalization of the Hamiltonian matrix. These functions are bound state-like, i.e., they are orthonormal in the ''Kronecker sense'' and have units of $[\text{Length}]^{-1/2}$.

The discrete, stick form of the total photofragmentation cross section is

$$\sigma_i(E;\alpha)\propto\sum_m |\langle\Phi_m(\alpha)|\boldsymbol{\mu}\cdot\mathbf{e}|\Psi_i(X)\rangle|^2\delta[E_m(\alpha)-E]. \tag{2.13}$$

Using a sufficiently small α value, a large density of states can be obtained. In such a case, Eq. (2.13) would provide a rather smooth function of E analogous to the accurate total cross section [Eq. (2.5)]. This procedure is, however, impractical since a very small α value involves working with extremely large Hamiltonian matrices. As Mandelshtam *et al.* have proposed,[17,19] it is better to work on a range of larger values of α and average. In this way, a mean cross section is defined as

$$\langle \sigma_i(E)\rangle \approx (\Delta\alpha)^{-1}\int_{\alpha_0}^{\alpha_0+\Delta\alpha} d\alpha\,\sigma_i(E;\alpha), \tag{2.14}$$

where a range of α values varying from α_0 to $\alpha_0+\Delta\alpha$ is considered. Inserting Eq. (2.13) into Eq. (2.14) and after a few operations,[17] the average cross section is written as

$$\langle \sigma_i(E)\rangle \approx (\Delta\alpha)^{-1}\sum_m \left|\frac{dE_m}{d\alpha}\right|^{-1}_{\alpha_m^*} |\langle \Phi_m(\alpha_m^*)|\boldsymbol{\mu}\cdot\mathbf{e}|\Psi_i(X)\rangle|^2, \tag{2.15}$$

where α_m^* is defined such that $E_m(\alpha_m^*)=E$; in other words, α_m^* is the value where the $E_m(\alpha)$ curve intersects the straight line E. Only α_m^* points belonging to the interval $[\alpha_0,\alpha_0+\Delta\alpha]$ are included in Eq. (2.15).

Stabilization calculations are easy to perform because they involve successively solving bound state-type problems for different values of a non-linear parameter α. They provide the so-called stabilization diagram, in which the eigenvalues E_m are plotted as functions of α (or vice versa). Quasibound states can be distinguished by their stable behavior, i.e., very small derivative $dE_m/d\alpha$ and, if the overlap involved in Eq. (2.15) not too small, they cause a ''bump'' in the photofragmentation cross section. Then, such resonances can be studied by inspection of nodal patterns of the corresponding wave functions. This analysis contributes to the understanding of the underlying dynamics in the fragmentation process. More details on the application of this method are given in the next section.

III. RESULTS AND DISCUSSION

Calculations have been conducted for the allowed transition in $HeBr_2$:$(X,\ v_0'=0,\ n'=0,\ J'^{p_i'}_{p_j'}=1^-_-)\rightarrow(B,\ v_0=45,\ n=0,\ J^{p_i}_{p_j}=0^+_+)$, already studied in a previous work.[1] $v_0(v_0')$ and $n(n')$ label approximate quantum numbers associated with the bromine stretch and vdW modes, respectively, of the $B(X)$ electronic state. In the expansion of Eq. (2.4), the size of the vibrational basis has been reduced, with respect to previous calculations,[1] to five vibrational channels ($v=42,43,44,45,46$). Using this smaller basis only leads to small quantitative differences in resonance positions and widths. Parameters of the interaction potentials and further computational details are given elsewhere.[1]

In the discussion of results, the following set of zero order diabatic states are considered

$$\Psi^0_{vn}=\chi_v\psi_{vn},\qquad \Psi^0_{vE}=\chi_v\psi_{vE}. \tag{3.1}$$

Ψ^0_{vn} and Ψ^0_{vE} are discrete and continuum eigenstates, respectively, of the projected Hamiltonian $H_v=P_vHP_v$, where $P_v=|\chi_v\rangle\langle\chi_v|$. The label n indicates the excitation in the vdW modes. Several perturbation approaches based on such zero order states have been successfully applied in this context to study direct dissociation (Fermi's Golden rule[32]) as well as in situations where an IVR mechanism mediates in the fragmentation[12,15,10]). The adequacy of this zero order picture in the present case is tested at the end of this section.

A. Coherence effects in the excitation process

In photofragmentation of rare-gas halogen complexes it is usually assumed that the initial state $(X,\ v_0'=0,\ n'=0)$ mainly couples radiatively with $(B,\ v_0,\ n=0)$ states of the different v_0 manifolds.[32,15] Such an assumption is supported by: a) no Fano-type resonances[33] have been observed,[31] so oscillator strength carried by zero order continuum states must be negligible, and b) transitions to states vibrationally excited in the vdW modes ($n>0$) are usually 1–2 orders of magnitude smaller than transitions to the ground vdW state.[31] It is possible that this simplification no longer holds in the case of the $HeBr_2$ photofragmentation. Indeed, Janda and co-workers[5] reported on an excitation band, blue-shifted to the main $v_0=8$ band, which was assigned to a progression in excited vdW modes. In a previous theoretical work,[1] however, we could not reproduce the relatively high intensity of such a band, concluding that more sophisticated X and B interaction potentials should be used in order to achieve a better agreement with experiment in this particular aspect.

Although here we continue to use the same interaction potentials,[1] it is worth testing the assumption of the ground vdW state being the only optically active state in a very different situation as it is found for very high initial excitations v_0. In this case, the zero order ''bright'' state $(v_0,\ n=0)$ faces discrete vdW-excited states belonging to the v_0-1 manifold, the latter states being ''candidates'' for doorway states in an IVR mechanism. It should be noted that, for $v_0>31$, FC factor $F(0,\ v_0-1)$ is larger (in absolute value) than $F(0,\ v_0)$ Ref. 34 (for example, $|F(0,44)|\approx 1.06|F(0,45)|$). So, although there were small overlaps between the vdW parts of the $(X,\ v_0)$ state and the (v_0-1) components of the B state [see first factor in Eq. (2.5)], this feature would show up in the total cross section.

Two types of ''artificial'' close-coupling calculations are presented in this section, together with the accurate one (already described in Sec. II B). In the first artificial calculation, it is assumed that FC factors involved in Eq. (2.6) are

$$F(0,v)=\langle\chi_v^B|\chi_0^X\rangle\,\delta_{v,v_0}, \tag{3.2}$$

with $v_0=45$. If the difference between the accurate results and the present approximation is negligible, it would mean that the excitation process is just dominated by the optically active state $(v_0=45,\ n=0)$. Complementarily, in the second ''artificial'' calculation it is assumed that

$$F(0,v)=\langle\chi_v^B|\chi_0^X\rangle(1-\delta_{v,v_0}). \tag{3.3}$$

This second scheme tests the possibility of direct optical transition to either discrete or continuum states of $v\neq 45$ manifolds.

In Fig. 1, total cross section is compared with the artificial calculations previously described. As can be seen, there is a noticeable difference between the full calculation and the approximate one where only states belonging to the $v=45$ manifold carry oscillator strength. Whereas positions of the

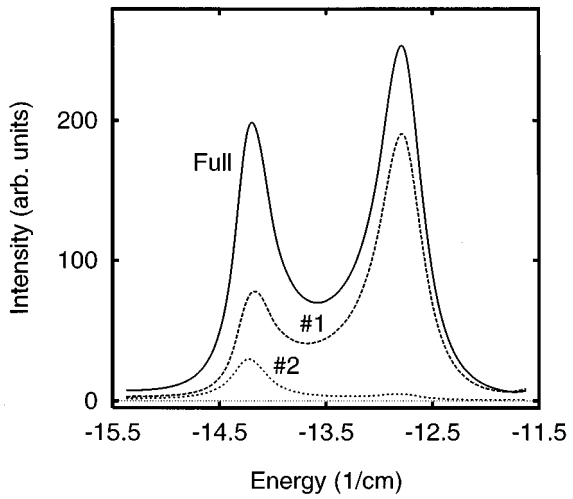

FIG. 1. Solid line: total cross section (in arbitrary units) as a function of energy (in cm^{-1}) for the $v_0=45$ level (''full'' calculation). Dashed line (#1): Same for the artificial Franck–Condon factors scheme of Eq. (3.2). Dotted line (#2): Same for the artificial Franck–Condon factors scheme of Eq. (3.3). Energy is referred to the $Br_2(B,\ v=45)$ level.

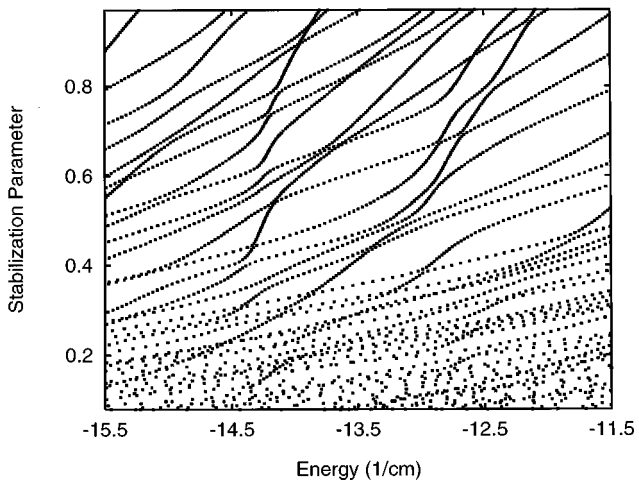

FIG. 2. Stabilization diagram for the $v_0=45$ level: stabilization parameter α versus discrete eigenvalues (in cm^{-1}) of the B state Hamiltonian referred to the $Br_2(B,\ v=45)$ energy level.

resonances are almost unchanged, the ratio between peak maxima are not well described within the approximation under consideration. By looking at the results of the second artificial calculation, it is noticed that states belonging to $v \neq 45$ manifolds do carry oscillator strength. In other words, the continuum wave functions [Eq. (2.4)] have components $\phi^{fE}_{v\neq 45}(R)$ with non-negligible amplitudes in the interaction region and thus, with a non-zero overlap with the ground state wave function [see Eq. (2.5)]. Moreover, the second artificial calculation gives a structured, resonant-like line shape, exhibiting two peaks whose positions and widths are roughly comparable to those of the ''exact'' calculation. This fact suggests that absorbing states are ''quasibound'' and, most probably, they correspond to the $v=44$ manifold. The larger intensity of the peak located at $E\approx -14.22$ cm^{-1} indicates that the corresponding resonance state has larger components on such quasibound states. On the other hand, it is clear from Fig. 1 that addition of #1 and #2 cross sections does not yield the full one. In other words, there is an important (constructive) interference effect between excitation paths leading to states belonging to either $v=45$ or $v \neq 45$ manifolds. In short, it has been shown here that to consider the $(v_0,\ n=0)$ state as the only optically active one is a poor description for the case of very high v_0 excitations in $HeBr_2$.

B. Stabilization line shapes

Stabilization calculations for obtaining the $v_0=45$ line shape were conducted using the same rovibrational channels as in the close-coupling calculations, i.e., 12 rotational and 5 vibrational basis functions. For the vdW stretching mode, R, 30 DVR functions were included, where the harmonic oscillator reference frequency was chosen to be that corresponding to the harmonic approximation of the interaction potential at the T-shape configuration, i.e., $\hbar\omega_0=22.45$ cm^{-1}. The scaling parameter α was varied from 0.0800 to 0.9710 in steps of 0.0045. The B state Hamiltonian matrix was successively diagonalized for the α-dependent basis set. The resulting stabilization diagram[16] (plot of α versus eigenvalues) is shown in Fig. 2. In this figure, it can be noticed that in the middle of a ''bath'' of unstable curves there are two stability regions around -14.22 and -12.81 cm^{-1}. Thus, this diagram shows that there are two quasibound states in the region explored. As $|dE_m/d\alpha|^{-1}$ terms have quite large values around the energies above indicated, two bumps in the total cross section are expected provided that the corresponding overlaps in Eq. (2.15) are not too small.

The calculation of the matrix elements involved in Eq. (2.15) has been simplified here. Instead of computing the X ground state and including $\boldsymbol{\mu}\cdot\mathbf{e}$ in the quadrature, the overlap between the zero order state $(v=45,\ n=0)$ and the stabilization wave functions, $|\langle\Phi^B_m(\alpha^*_m)|\Psi^0_{v=45,\ n=0}\rangle|^2$, is computed. This calculation can be directly compared with the above-reported artificial close-coupling calculation where the only non-zero FC factor is $F(0,45)$ [Eq. (3.2)]. In fact, it has been checked that close-coupling calculations performed a) using the approximation given by Eq. (3.2), and b) taking into account the simplifications mentioned above, give identical results after scaling by a global factor.

In Fig. 3, the stabilization line shape is compared with the corresponding scaled close-coupling one. It can be seen that the stabilization method reproduces fairly well the accurate calculations. Positions and widths of the resonances extracted from either calculation are almost identical, and the ratio between maxima of the two peaks is well described. The two calculations only differ in the intermediate region. This is due to the fact that a larger range in the scaling parameter α should be used. This was not done because a much larger basis set would be needed to achieve full convergence.

The previous result indicates that stabilization calculations give a good simulation of photofragmentation cross

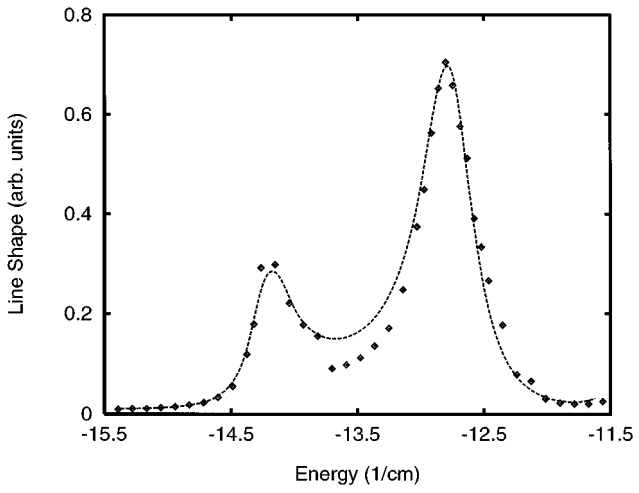

FIG. 3. Stabilization cross section (dashed line) versus energy, compared with the close-coupling calculation (solid line) for the $v_0=45$ level. See text for more details.

sections, although so far it is not a competitive method in comparison with the more efficient close-coupling approach. However, within the close-coupling method it is a difficult task to obtain quasibound wave functions involved in the predissociation dynamics. Stabilization calculations, in turn, allow one to examine quasibound wave functions, which is the subject of the next paragraph.

C. Resonance analysis from stabilization calculations

In order to facilitate the discussion below, we will refer to the resonances located around -14.22 and -12.81 cm^{-1} (see Fig. 3) as L (left) and R (right) resonances, respectively. Several magnitudes have been obtained from the stabilization wave functions obtained at a given value of α. First, the density function for the interhalogen stretch (indexes J, M, Ω, p_i and p_j are dropped since they have fixed values throughout),

$$\delta_m(r;\alpha)=\int |\Phi_m(\alpha)|^2 \sin\theta \mathrm{d}\theta \mathrm{d}R$$

$$=\sum_{jk} |\sum_{v} b^m_{vkj}(\alpha)\chi_v(r)|^2. \tag{3.4}$$

The density function for the vdW degrees of freedom, R and θ, is also extracted:

$$\rho_m(R,\theta;\alpha)=\sin\theta \int |\Phi_m(\alpha)|^2 \mathrm{d}r$$

$$=\sum_{v} \rho^v_m(R,\theta;\alpha), \tag{3.5}$$

where ρ^v_m is the v component of such a density function:

$$\rho^v_m(R,\theta;\alpha)=\left|\sum_{k,j} b^m_{vkj}(\alpha)\varphi_k(R;\alpha)\Theta_j(\theta)\right|^2 \sin\theta. \tag{3.6}$$

Moreover, weights of a given halogen vibrational state are computed:

TABLE I. Energies (in cm^{-1}) of the bound zero order states Φ^0_{vn} referred to the $Br_2(B,\ v=45)$ level. Only states corresponding to the $p_j=+1$ parity block are displayed here.

n	$v=42$	$v=43$	$v=44$	$v=45$	$v=46$
0	−51.8722	−36.1084	−22.2174	-10.1586	0.2802
1	−45.9421	−30.4457	−16.8649	−5.1861	4.8156
2	−44.3510	−28.8775	−15.3148	−3.6563	6.3322
3	−41.8212	−26.4051	−12.9008	−1.3020	8.6263

$$w^{v'}_m(\alpha)=\sum_{kj} |b^m_{v'kj}(\alpha)|^2=\int \rho^{v'}_m(R,\theta;\alpha)d\theta dR. \tag{3.7}$$

In addition, a zero order basis set, analogous to that given in Eq. (3.2), is considered

$$\Phi^0_{vn}(\alpha)=\chi_v\phi_{vn}(\alpha), \tag{3.8}$$

where the only difference with respect to the basis of Eq. (3.1) is that, here, all wave functions are square-integrable since they are obtained from diagonalization of the Hamiltonians H_v defined above. Then, some zero order states represent discretized continua and thus they explicitly depend on the stabilization parameter. In order to assign the stabilization quasibound states to quantum numbers within this framework, overlaps with zero-order states are obtained:

$$w^{vn}_m(\alpha)=|\langle\Phi^0_{vn}(\alpha)|\Phi_m(\alpha)\rangle|^2, \tag{3.9}$$

satisfying $\Sigma_n w^{vn}_m=w^v_m$.

Before presenting the results corresponding to the $v_0=45$ level, it is worth describing what happens at the simpler $v_0=25$ case, which is in the $\Delta v=-1$ regime and where effective couplings are weaker. Perturbation approaches based on zero order states defined above become highly accurate and, in this way, dissociation can be viewed as a simple mechanism where the $\Psi^0_{v=25,n=0}$ state couples directly to the continua of the $v=24$ manifold. In fact, the zero-order resonance position, $E^0=-13.29$ cm^{-1}, is close to the exact value $E=-13.32$ cm^{-1}, and the Fermi's Golden Rule rate,[1] $\Gamma^0=0.189$ cm^{-1}, compares satisfactorily with the close-coupling result, $\Gamma=0.191$ cm^{-1}. Also, stabilization calculations performed in this case yield resonance line shapes in perfect agreement with the close-coupling ones. In the corresponding stabilization diagram, an almost straight line at the resonance position is found crossed by multiple curves corresponding to very unstable continua. As expected, wave functions corresponding to the stable resonance curve are very similar, and almost independent of the stabilization parameter, to the zero-order state ($v=25,\ n=0$). In these stable regions, weights of vibrational states $v\neq 25$ are almost negligible, and only when a crossing with an unstable curve occurs, larger $v\neq 25$ components are found as there is a mixing between the quasibound state and continuum states (which have their largest components on $v=24$).

A more complex situation is expected for $v_0=45$ since the $\Delta v=-1$ channel is closed and effective couplings are much stronger. In Table I, the set of bound zero-order energies, referred to the $Br_2(v=45)$ level, are shown. Note that

TABLE II. Weights of the different v components for some stabilization states corresponding to the L resonance (at $E=-14.2158\ cm^{-1}$). See text for details on the selection criteria. For each α_l value, the eigenvalue E_m and its ordinal number m are listed. For each v, the leading zero order vdW levels, n^*, as well as their corresponding weights, $\omega_m^{vn^*}$, are presented. (Except for the $v=46$ case, where these weights are already very small.)

l	α_l	m	$E_m\ (cm^{-1})$	$\omega_m^{v=42}$	n^*	$\omega_m^{v=42n^*}$	$\omega_m^{v=43}$	n^*	$\omega_m^{v=43n^*}$	$\omega_m^{v=44}$	n^*	$\omega_m^{v=44n^*}$	$\omega_m^{v=45}$	n^*	$\omega_m^{v=45n^*}$	$\omega_m^{v=46}$
1	0.4715	67	−14.2845	0.0332	43	0.0167	0.1406	19	0.0368	0.7169	3	0.5418	0.1076	0	0.0893	0.0017
2	0.6065	64	−14.2158	0.3333	40	0.2716	0.1557	19	0.0564	0.3819	3	0.2872	0.1272	0	0.1069	0.0020
3	0.6605	63	−14.1968	0.0333	42	0.0130	0.3311	18	0.1336	0.5265	3	0.3813	0.1075	0	0.0910	0.0016
4	0.7145	62	−14.2400	0.0708	39	0.0370	0.2801	18	0.2081	0.4661	3	0.3738	0.1804	0	0.1506	0.0039
5	0.7505	61	−14.1931	0.0772	39	0.0442	0.1862	18	0.0804	0.5176	3	0.4088	0.2159	0	0.1825	0.0031
6	0.7955	60	−14.1480	0.2423	38	0.2172	0.1278	16	0.0424	0.5227	3	0.4149	0.1056	0	0.0896	0.0015

only states of the $j=even$ parity block are displayed here. Apart from discrete-continuum or more complex interactions, one would expect the $(v=45,\ n=0)$ zero-order level to couple with the bound states of the $v=44$ manifold. The zero-order resonance position is thus given by the energy of the $(v=45,\ n=0)$ state, $E^0=-10.157\ cm^{-1}$. Notice how far this estimation is from the accurate L and R resonance positions (-14.22 and $-12.81\ cm^{-1}$, respectively). Moreover, it should be stressed that, within this approximation, the $\Delta v=-1$ channel would be open ($v=44$ threshold is at $E=-11.65\ cm^{-1}$). It is foreseen that, in this regime, such a zero order scheme hardly gives a reliable picture of the intramolecular dynamics, but rather it must result from a complex configuration-interaction effect.

Weights and density functions were obtained for several selected values of α, denoted as α_l $(l=1,2,\ldots)$. They were chosen following two criteria: a) one of the corresponding eigenvalues is very close to one of the resonance energies, $E_m(\alpha_l)\approx E_L$ or E_R, and b) $E_m(\alpha)$ is a fairly smooth and stable function around α_l. The corresponding wave functions represent the L and R quasibound states involved in the process. Weights of different v states are presented in Tables II and III, for resonances L and R, respectively. Also, the leading zero-order components, n^*, (those having the largest weight, $w_m^{vn^*}$, at each v) as well as the corresponding weights are reported in those Tables. As can be seen, resonance L is dominated by the $(v=44,\ n=3)$ state, whereas resonance R has its largest weight on $(v=45,\ n=0)$. Note, however, that in general $w_m^{vn^*}<<w_m^v$, i.e., other components (v,n) different to the leading one (v,n^*) are important at each v. In addition, note that $v=42,43$ continuum states have very important weights. It is a bit surprising that, for some α values apparently rather far from a crossing region, such weights are so large (compare with the $v_0=25$ case discussed above). Nevertheless, whereas $(v=45,\ n=0)$ and $(v=44,\ n=3)$ states contribute to the resonances all along the stabilization diagram, n^* for $v<44$ varies with α (it has been checked that different n labels do involve distinct nodal structures in the corresponding zero-order states). Thus, although continuum $v=42,43$ components are always very important, they appear as more ''spurious'' than the discrete $v=44,45$ ones. Therefore, and in spite of many other nonnegligible contributions, it can be recognized that the $(v=44,\ n=3)$ and $(45,0)$ zero order discrete states neatly describe the stable portion of these resonances. Actually, a different zero order separation of the Hamiltonian should be considered in order to represent the interaction levels in terms of simple ''bright'' and ''dark'' states as required within the frame of sparse IVR models.[12–15] On the other hand, the usual parametrization on the vibration of the diatomic partner leads to the use of the present zero order separation. In this context one may identify the L and R resonances mainly to correspond to $(v=44,\ n=3)$ and $(45,0)$ zero order states, respectively. Note that this assignment is in accord with the strategy adopted in the previous work,[1] i.e., to consider the highest peak found in the corresponding line shape calculations as representative of the v_0 level under study. However, such an agreement can be merely casual. Because of the presence of the two factors determining the behavior of the cross-section, Eq. (2.15), it would be possible that the maximum peak be due to a different zero order state contributing with very high derivatives. In this sense, quasibound state analysis through stabilization calculations provides a way to accurately assign v_0-dependent magnitudes as energy shifts and widths.

Some of these findings are better displayed in a pictorial way. Density functions and weights w_m^{vn} are reported for two values of α corresponding to $l=1$ and $l=2$ of Tables II and III, respectively. In Figs. 4 and 5, and for resonances L and R, respectively, are presented: a) interhalogen density functions (solid lines); b) $v=45$ component of the vdW density functions; c) the same for $v=44$; and d) weights of the different zero-order configurations, (v,n). Figs 4(a) and 5(a) illustrate that the bromine vibration, within the complex, is no longer well defined. For the sake of comparison, density functions for the isolated bromine at vibrational states $v=44$ and $v=45$ (dashed lines) are depicted in Figs. 4(a) and 5(a), respectively. For both resonances, it can be seen that the highest probability density is reached at very large interhalogen distances. The short range part of the density functions exhibit a better-defined nodal structure. This is due to the strong similarity that highly excited wave functions have there. On the contrary, at long distances pure vibrational functions do differ and the result of the addition given by Eq. (3.4) is a less structured and very broad probability density. In Figs. 4(b) and 5(b) it is shown that both $v=45$ components of L and R resonance states look like ground vdW states. Figs. 4(c) and 5(c) display nodal patterns of the

TABLE III. Same as in Table II, for the R resonance at $E=-12.8104$ cm^{-1}.

l	α_l	m	E_m (cm^{-1})	$\omega_m^{v=42}$	n^*	$\omega_m^{v=42n^*}$	$\omega_m^{v=43}$	n^*	$\omega_m^{v=43n^*}$	$\omega_m^{v=44}$	n^*	$\omega_m^{v=44n^*}$	$\omega_m^{v=45}$	n^*	$\omega_m^{v=45n^*}$	$\omega_m^{v=46}$
1	0.4040	73	−12.9171	0.0826	45	0.0399	0.2964	24	0.0897	0.3022	3	0.0855	0.3755	0	0.3406	0.0070
2	0.4265	73	−12.8181	0.0808	44	0.0401	0.3100	22	0.1431	0.2782	3	0.1100	0.3245	0	0.2954	0.0065
3	0.5525	70	−12.9309	0.0367	42	0.0167	0.3310	22	0.1167	0.1660	3	0.1004	0.4583	0	0.4146	0.0080
4	0.7145	67	−12.7775	0.1159	41	0.0883	0.2718	20	0.1577	0.2941	3	0.1752	0.3120	0	0.2849	0.0062
5	0.7325	67	−12.7363	0.1630	41	0.1378	0.2244	20	0.0944	0.2901	3	0.1722	0.3162	0	0.2895	0.0062
6	0.7955	66	−12.7483	0.1636	41	0.0995	0.2391	20	0.1284	0.3022	3	0.1614	0.1636	0	0.2665	0.0051

$v=44$ components. They roughly correspond to bending excited vdW states, although stretch excitations are noticeable near the perpendicular configuration ($\theta\approx\pi/2$). It is also observed that, whereas $v=45$ density functions of L and R resonances are quite similar, the $v=44$ ones present a different nodal structure around the equilibrium configuration. In Figs. 4(d) and 5(d), components w^{vn} of L and R resonances on the zero order configurations are depicted. Apart from $v=42,43$ continuum state contributions, it is seen again that the dominant zero-order states are ($v=45$, $n=0$) and

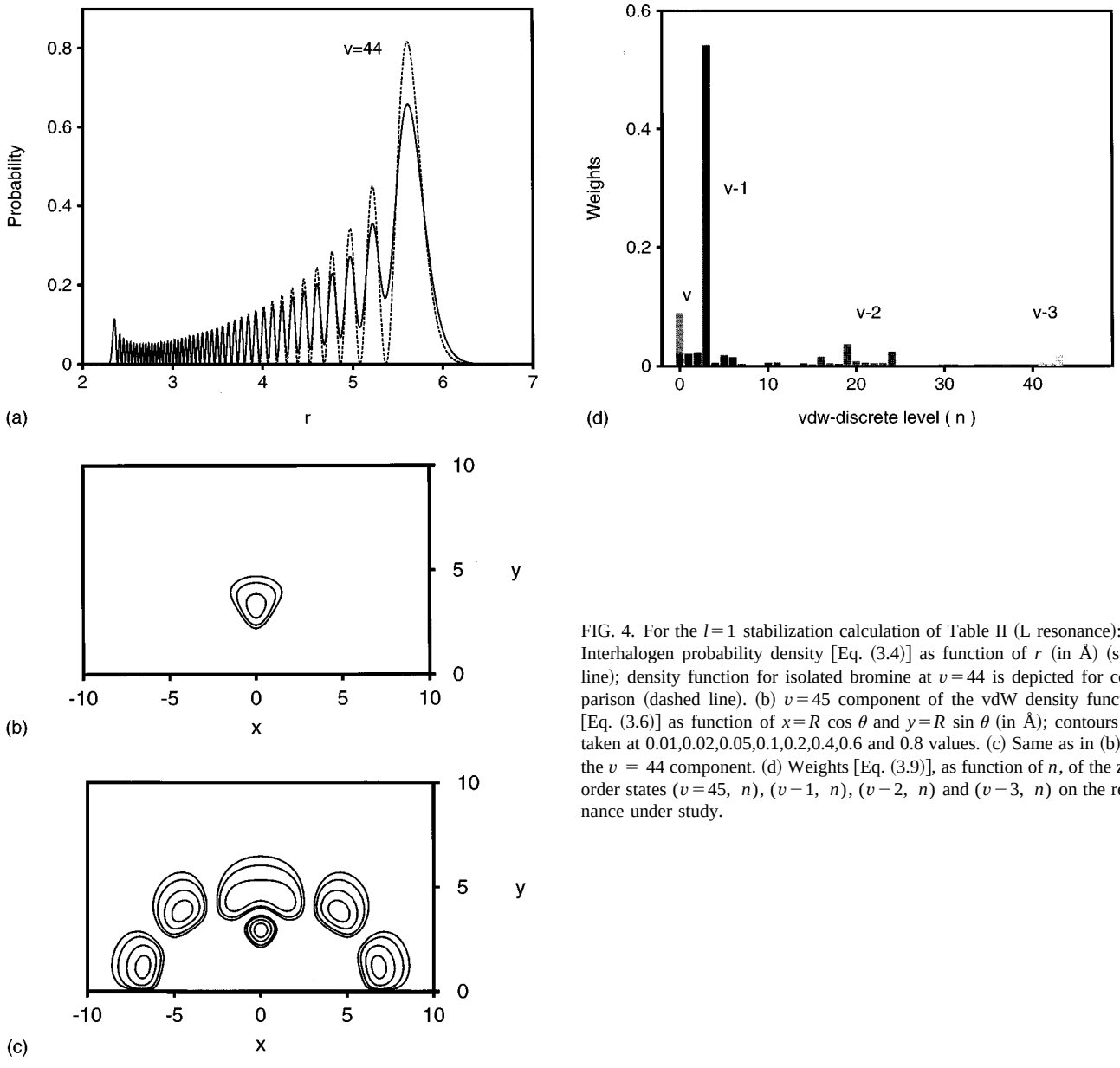

FIG. 4. For the $l=1$ stabilization calculation of Table II (L resonance): (a) Interhalogen probability density [Eq. (3.4)] as function of r (in Å) (solid line); density function for isolated bromine at $v=44$ is depicted for comparison (dashed line). (b) $v=45$ component of the vdW density function [Eq. (3.6)] as function of $x=R\cos\theta$ and $y=R\sin\theta$ (in Å); contours are taken at 0.01,0.02,0.05,0.1,0.2,0.4,0.6 and 0.8 values. (c) Same as in (b) for the $v=44$ component. (d) Weights [Eq. (3.9)], as function of n, of the zero order states ($v=45$, n), ($v-1$, n), ($v-2$, n) and ($v-3$, n) on the resonance under study.

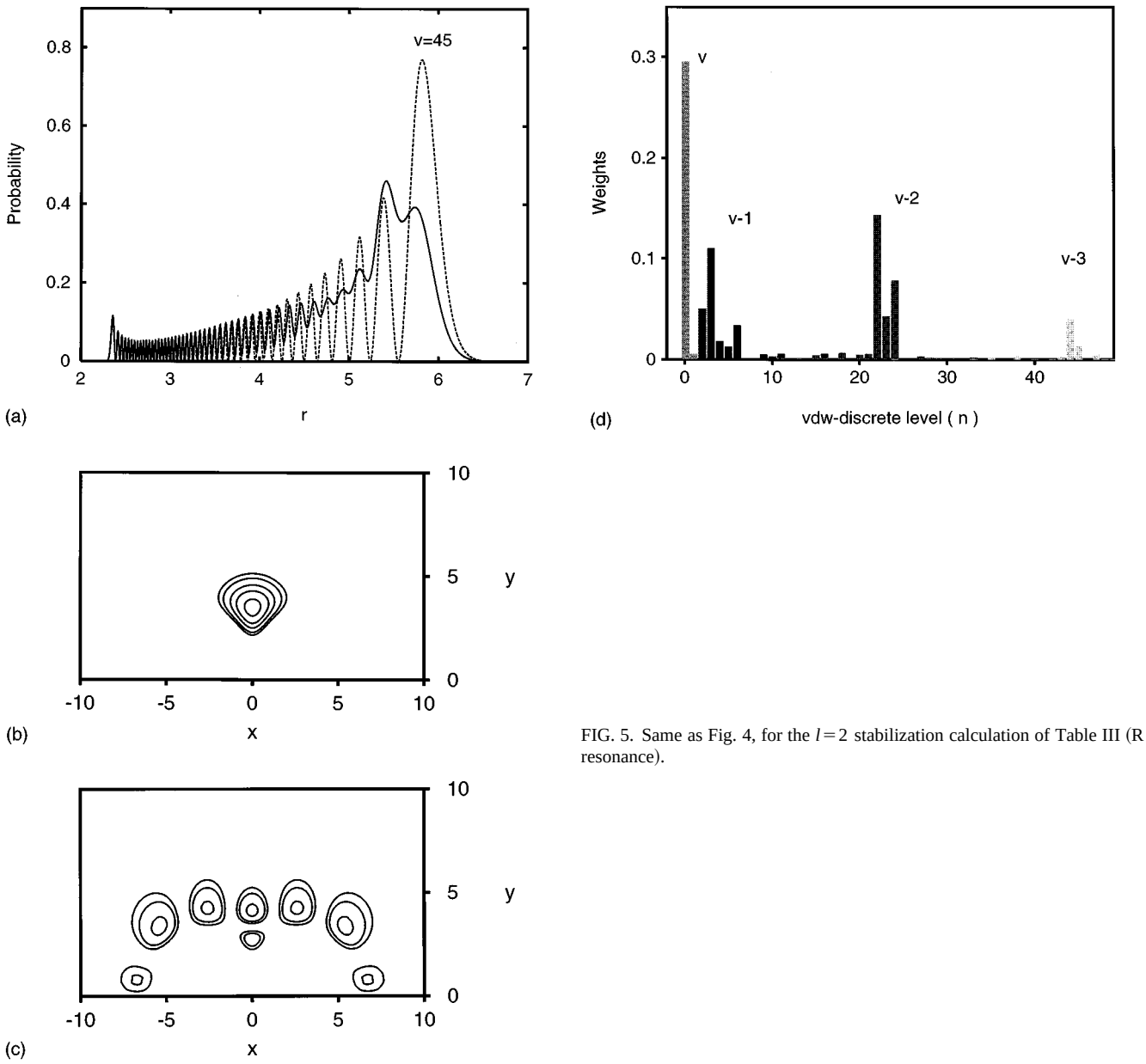

FIG. 5. Same as Fig. 4, for the $l=2$ stabilization calculation of Table III (R resonance).

$(v=44,\ n=3)$ but, nevertheless, there are other zero order states $(v=44,\ n)$ contributing to resonances. This effect is stronger in the case of the R resonance, where states $(v=44,\ n=2)$ and $(v=44,\ n=6)$ bring non-negligible weights [note that $(v=44,\ n=6)$ is a continuum state]. The latter contributions are the origin of the differences in nodal structures of $v=44$ L and R density functions. Finally, in Fig. 6, zero-order $(v=45,\ n=0)$ (6a) and $(v=44,\ n=3)$ (6b) vdW density functions are shown. Zero order state $(v=45,\ n=0)$ and the $v=45$ components of both resonances [Figs. 4(b) and 5(b)] are fairly similar, although the latter are much more localized as a result of an overall configuration interaction effect. On the other hand, the $(v=44,\ n=3)$ zero order state exhibits a strong similarity with the $v=44$ component of the L resonance [compare Figs. 4(c) and 6(b)], but not with the same component of the R resonance, as expected in view of histograms of Figs. 4(d) and 5(d).

IV. CONCLUSIONS

The fragmentation dynamics of $HeBr_2(B,\ v_0=45)$ has been studied by means of stabilization as well as close-coupling methods. Stabilization total cross sections agree with the close coupling ones, although the former is still a less efficient method. Stabilization calculations, however, allow a closer inspection of the underlying dynamics. Furthermore, the stabilization formula for the total cross section [Eq. (2.15), see also Ref. 19] would be useful to study fragmentation processes where more than one bond can be bro-

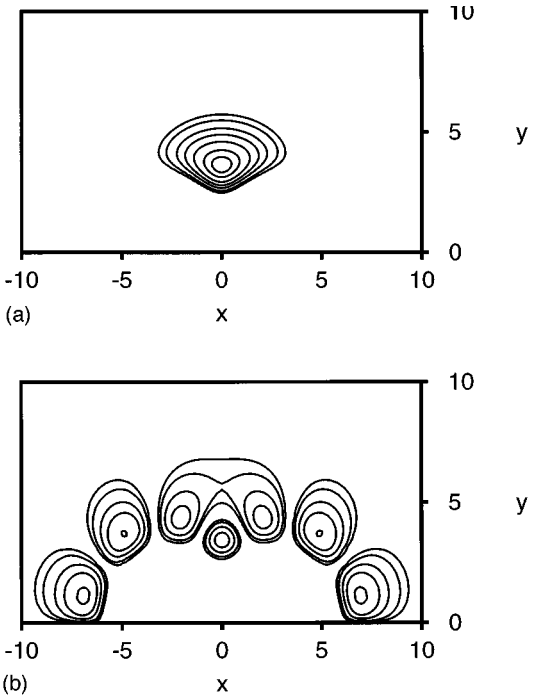

FIG. 6. Contour plots of the ($v=45$, $n=0$) (a) and ($v=44$, $n=3$) (b) zero- order vdW density functions. Eigenvalues of the corresponding states are indicated in Table I. ($x=R\cos\theta$ and $y=R\sin\theta$ are given in Å). Contour values are those indicated in Fig. 4(b).

ken (for instance two rare gases-halogen systems[35–37]) since in such situations simple close-coupling expansions become impractical.

It is found that $HeBr_2$ at high v_0 excitations is a strongly coupled system, where it is difficult to assign resonances to simple quantum numbers either in stretch (r and R) or bending modes. In an approximate way, intramolecular dynamics in $HeBr_2(B,\ v_0=45)$ proceeds via coupling of the ($v=45$, ground) zero-order state, which carries the largest oscillator strength, with the ($v=44$, $n=3$) state corresponding to a vdW bending excitation. There are, however, non-negligible couplings with bound and continuum states of $v=44$ and other v manifolds. Moreover, doorway states do not appear to be as ''dark'' as could be supposed. By performing some artificial calculations within the close-coupling approach, it has been shown that in the excitation process a coherent state is prepared [although ($v=45$, ground) still carries the largest component] and thus interference effects in the excitation spectra are significant. Relatively simple IVR models which have been successfully used in related systems (such as, e.g., $ArCl_2$ Refs. 12,13,15) might be applied only by starting with a zero-order separation of the Hamiltonian different from the (standard) used here.

One of the main characteristics of rare gas-halogen complexes is that the weak vdW interaction does not perturb significantly the halogen vibrational motion or, in other words, the halogen vibration is usually a fairly good quantum number. We conclude in this work that this is not any longer the situation for the $HeBr_2(B,\ v_0=\text{high})$ dynamics. As Br_2 and $He-Br_2$ vibrational frequencies become closer, the halogen subunit does not retain its identity. The complex could be seen as a very ''loose'' molecule where average internuclear distances are quite large. To obtain more insight into the intramolecular dynamics of $HeBr_2(v_0=\text{high})$, some other perturbation schemes taking into account the latter arguments should be devised.

ACKNOWLEDGMENTS

We wish to thank O. Roncero for the useful discussions maintained. Also, the valuable comments of A. Buchachenko are highly appreciated. This work has been partially supported by the DGICYT Grant PB95-0071 (Spain) and the European Union Grant CI1*-CT94-0128.

[1] T. González-Lezana, M. I. Hernández, G. Delgado-Barrio, A. A. Buchachenko, and P. Villarreal, J. Chem. Phys. **105**, 7454 (1996).
[2] L. J. van de Burgt, J. P. Nicolai, and M. C. Heaven, J. Chem. Phys. **81**, 5514 (1984).
[3] D. G. Jahn, S. G. Clement, and K. C. Janda, J. Chem. Phys. **101**, 283 (1994).
[4] N. Sivakumar, J. I. Cline, C. R. Bieler, and K. C. Janda, Chem. Phys. Lett. **147**, 561 (1988).
[5] D. G. Jahn, W. S. Barney, J. Cabalo, S. G. Clement, A. Rohrbacher, T. J. Slotterback, J. Williams, K. C. Janda, and N. Halberstadt, J. Chem. Phys. **104**, 3501 (1996).
[6] O. Roncero, J. Campos-Martínez, A. M. Cortina, P. Villarreal, and G. Delgado-Barrio, Chem. Phys. Lett. **148**, 62 (1988).
[7] J. J. Breen, D. M. Willberg, M. Gutmann, and A. H. Zewail, J. Chem. Phys. **93**, 9180 (1990).
[8] M. L. Burke and W. Klemperer, J. Chem. Phys. **98**, 6642 (1993).
[9] S. K. Gray and O. Roncero, J. Phys. Chem. **99**, 2512 (1995).
[10] O. Roncero and S. K. Gray, J. Chem. Phys. **104**, 4999 (1996).
[11] D. D. Evard, C. R. Bieler, J. I. Cline, N. Sivakumar, and K. C. Janda, J. Chem. Phys. **89**, 2829 (1988).
[12] N. Halberstadt, J. A. Beswick, O. Roncero, and K. C. Janda, J. Chem. Phys. **96**, 2404 (1992).
[13] N. Halberstadt, S. Serna, O. Roncero, and K. C. Janda, J. Chem. Phys. **97**, 341 (1992).
[14] K. C. Janda, N. Halberstadt, and O. Roncero (preprint).
[15] O. Roncero, P. Villarreal, G. Delgado-Barrio, N. Halberstadt, and K. C. Janda, J. Chem. Phys. **99**, 1035 (1993).
[16] A. U. Hazi and H. S. Taylor, Phys. Rev. A **1**, 1109 (1970).
[17] V. A. Mandelshtam, T. R. Ravuri, and H. S. Taylor, Phys. Rev. Lett. **70**, 1932 (1993).
[18] M. I. Hernández and D. C. Clary, J. Chem. Phys. **101**, 2779 (1994).
[19] V. A. Mandelshtam, T. R. Ravuri, and H. S. Taylor, Phys. Rev. A **48**, 818 (1993).
[20] V. A. Mandelshtam and H. S. Taylor, J. Chem. Phys. **99**, 222 (1993).
[21] V. A. Mandelshtam, H. S. Taylor, V. Ryaboy, and N. Moiseyev, Phys. Rev. A **50**, 2764 (1994).
[22] V. Ryaboy, N. Moiseyev, V. A. Mandelshtam, and H. S. Taylor, J. Chem. Phys. **101**, 5677 (1994).
[23] V. A. Mandelshtam, H. S. Taylor, C. Jung, H. F. Bowen, and D. J. Kouri, J. Chem. Phys. **102**, 7988 (1995).
[24] (a) T. Seideman, J. Chem. Phys. **98**, 1989 (1993); (b) R. C. Mayrhofer and J. M. Bowman, *ibid.* **100**, 7299 (1994); (c) **102**, 5598 (1995).
[25] S. C. Tuker and D. G. Truhlar, J. Chem. Phys. **86**, 6251 (1987).
[26] R. S. Salzgeber, U. Manthe, Th. Weiss, and Ch. Schlier, Chem. Phys. Lett. **249**, 237 (1996).
[27] O. Roncero, J. A. Beswick, N. Halberstadt, P. Villarreal, and G. Delgado-Barrio, J. Chem. Phys. **92**, 3348 (1990).
[28] J. I. Cline, B. P. Reid, D. D. Evard, N. Sivakumar, N. Halberstadt, and K. C. Janda, J. Chem. Phys. **89**, 3535 (1988).
[29] L. Fox, *The Numerical Solution of Two-Point Boundary Value Problems in Ordinary Differential Equations* (Oxford University Press, London, 1957).

[30] O. Roncero (private communication).
[31] D. H. Levy, Adv. Chem. Phys. **47**, 323 (1981).
[32] J. A. Beswick and J. Jortner, Adv. Chem. Phys. **47**, 363 (1981).
[33] U. Fano, Phys. Rev. **124**, 1866 (1961).
[34] R. F. Barrow, T. C. Clark, J. A. Coxon, and K. K. Yee, J. Mol. Spectros. **51**, 428 (1974).
[35] M. Gutmann, D. M. Willberg, and A. H. Zewail, J. Chem. Phys. **97**, 8048 (1992).
[36] O. Roncero, G. Delgado-Barrio, M. I. Hernández, J. Campos-Martínez, and P. Villarreal, Chem. Phys. Lett. **246**, 187 (1995).
[37] J. Campos-Martínez, M. I. Hernández, O. Roncero, P. Villarreal, and G. Delgado-Barrio, Chem. Phys. Lett. **246**, 197 (1995).